3866 *Inorg. Chem.* **2010**, *49*, 3866–3880
DOI: 10.1021/ic1000073

Inorganic Chemistry
Article

Is $[FeO]^{2+}$ the Active Center Also in Iron Containing Zeolites? A Density Functional Theory Study of Methane Hydroxylation Catalysis by Fe-ZSM-5 Zeolite

Angela Rosa,*,† Giampaolo Ricciardi,*,† and Evert Jan Baerends*,‡,§

†*Dipartimento di Chimica, Università della Basilica, Via N. Sauro 85, 85100 Potenza, Italy,* ‡*Dep. of Chemistry, Pohang Univ. of Science and Technology, Pohang 790-784, South-Korea, and* §*Theoretische Chemie, Vrije Universiteit Amsterdam, De Boelelaan 1083, 1081 HV Amsterdam, The Netherlands*

Received January 2, 2010

Arguments are put forward that the active α-oxygen site in the Fe-ZSM-5 catalyst consists of the FeO^{2+} moiety. It is demonstrated that this zeolite site for FeO^{2+} indeed obeys the design principles for high reactivity of the FeO^{2+} moiety proposed earlier: a ligand environment consisting of weak equatorial donors (rather oxygen based than nitrogen based) and very weak or absent *trans* axial donor. The α-oxygen site would then owe its high reactivity to the same electronic structure features that lends FeO^{2+} its high activity in biological systems, as well as in the classical Fenton chemistry.

Introduction

Ironoxo compounds play a very important role in the catalysis of many oxidation reactions, ranging from the classical Fenton reaction to biological systems like the porphyrin based P450 enzymes,[1,2] taurine/α-ketoglutarate dioxygenase (TauD),[3,4] and methane monooxygenase (MMO).[5,6] In many cases the FeO^{2+} unit is the postulated active moiety. This is the case in P450s, TauD, the synthesized biomimetic analogues[7] like $[Fe^{IV}(O)(N_4Py)]^{2+}$ and $[Fe^{IV}(O)(TMC)(CH_3CN)]^{2+}$ (N4Py = *N*,*N*-bis(2- pyridylmethyl)-*N*-bis(2-pyridyl)methylamine, TMC = 1,4,8,11-tetramethyl-1,4,8,11-tetraazacyclotetradecane), and the recently synthesized pentaaqua complex of FeO^{2+}.[8] Also in the Fenton chemistry $(H_2O)_5FeO^{2+}$ has been found to be the active intermediate in electronic structure density functional theory (DFT) calculations[9,10] and in Car−Parrinello MD simulations of the reaction of H_2O_2 with Fe^{2+} in water solvent,[11,12] but the most recent experimental work[8] favors $OH^{\cdot}$ radical rather than FeO^{2+} as reaction intermediate (see ref 13 for an alternative experimental point of view). The reactivity of FeO^{2+} will be determined by the ligand environment. It has been emphasized that the fact that FeO^{2+} may have different spin states is crucial for a complete understanding of the reactivity in the various cases, the high-spin quintet ($S = 2$) being notably more active than the triplet ($S = 1$) state. The quintet may not be the ground state initially in, for example, the reactants complex, but crossover to the quintet state may then offer passage over a lower barrier, compare the two-state reactivity documented in many cases by Shaik and co-workers.[14,15] It is however important to note that the triplet to quintet conversion is only one of the electronic structure factors that determine the FeO^{2+} reactivity. In Figure 1 we give the orbital energy level diagrams[16] of two prototype systems, the pentaamine complex, representative of systems such as $[Fe^{IV}(O)(N_4Py)]^{2+}$ and $[Fe^{IV}(O)(TMC)(CH_3CN)]^{2+}$, and the pentaaqua complex, present in the Fenton chemistry and representative of the oxygen donor ligand environment in some of the biological systems like MMO and TauD. The diagrams contain the iron-oxo bonding levels of σ and π type (1π and 2σ) as lowest levels (ca. 50% oxygen character, but

*To whom correspondence should be addressed. E-mail: angela.rosa@unibas.it (A.R.), rg010sci@unibas.it (G.R.), ej.baerends@few.vu.nl (E.J.B.).

(1) Meunier, B.; de Visser, S. P.; Shaik, S. *Chem. Rev.* **2004**, *104*, 3947.
(2) Schöneboom, J. C.; Cohen, S.; Lin, H.; Shaik, S.; Thiel, W. *J. Am. Chem. Soc.* **2004**, *126*, 4017.
(3) Price, J. C.; Barr, E. W.; Tirupati, B., Jr.; J. M., B.; Krebs, C. *Biochemistry* **2003**, *42*, 7497.
(4) Hoffart, L. M.; Barr, E. W.; Guyer, R. B.; Bollinger, J. M., Jr.; Krebs, C. *Proc. Natl. Acad. Sci. U.S.A.* **2006**, *103*, 14738.
(5) Solomon, E. I.; Sundaram, U. M.; Machonkin, T. E. *Chem. Rev.* **1996**, *96*, 2563.
(6) Que, L.; Dong, Y. H. *Acc. Chem. Res.* **1996**, *29*, 190.
(7) Rohde, J.-U.; In, J.-H.; Lim, M. H.; Brennessel, W. W.; Bukowski, M. R.; Stubna, A.; Münck, E.; Nam, W.; Que, L., Jr. *Science* **2003**, *299*, 1037.
(8) Pestovsky, O.; Stoian, S.; Bominaar, E. L.; Shan, X.; Munck, E.; Que, L.; Bakac, A. *Angew. Chem., Int. Ed.* **2005**, *44*, 6871.
(9) Buda, F.; Ensing, B.; Gribnau, M. C. M.; Baerends, E. J. *Chem.—Eur. J.* **2001**, *7*, 2775.
(10) Buda, F.; Ensing, B.; Gribnau, M. C. M.; Baerends, E. J. *Chem.—Eur. J.* **2003**, *9*, 3436.
(11) Ensing, B.; Buda, F.; Blöchl, P. E.; Baerends, E. J. *Phys. Chem. Chem. Phys.* **2002**, *4*, 3619.
(12) Ensing, B.; Buda, F.; Gribnau, M. C. M.; Baerends, E. J. *J. Am. Chem. Soc.* **2004**, *126*, 4355.
(13) Kremer, M. *Int. J. Chem. Kin.* **2006**, *38*, 725.
(14) Shaik, S.; Filatov, M.; Schröder, D.; Schwarz, H. *Chem.—Eur. J.* **1998**, *4*, 193.
(15) Hirao, H.; Kumar, D.; Que, L.; Shaik, S. *J. Am. Chem. Soc.* **2006**, *128*, 8590.
(16) Bernasconi, L.; Louwerse, M. J.; Baerends, E. J. *Eur. J. Inorg. Chem.* **2007**, 3023.

 Published on Web 03/21/2010

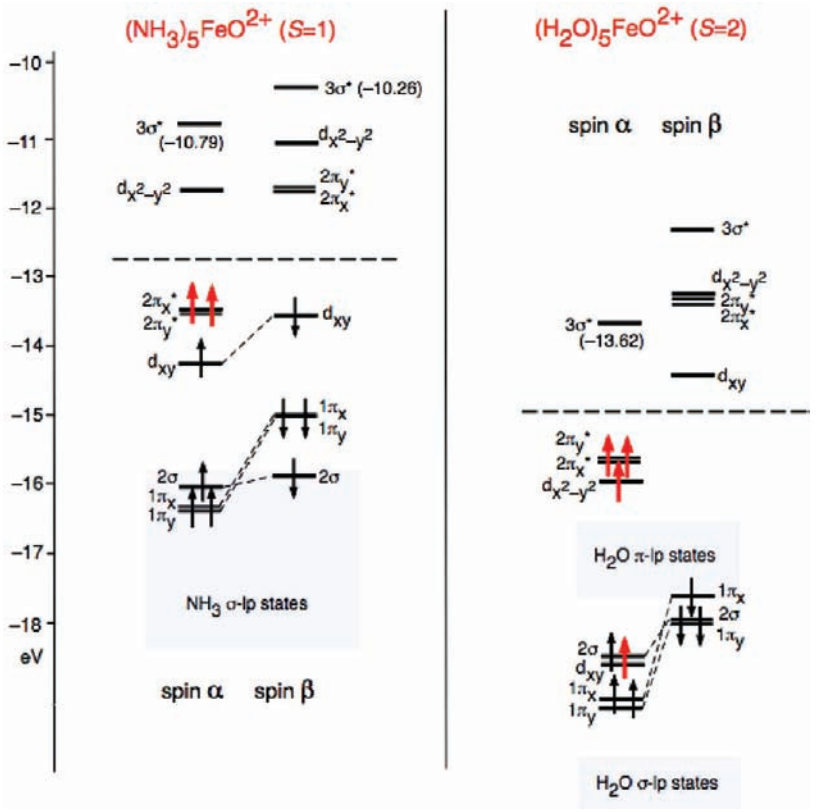

Figure 1. Orbital energy diagram showing the strong stabilization of the levels of the all oxygen donor ligand environment of $(H_2O)_5FeO^{2+}$(S = 2) compared to the all nitrogen donor ligand environment of $(NH_3)_5FeO^{2+}$ (S = 1). Unpaired electrons are indicated in red. Spin α orbital levels are stabilized by the exchange field compared to the corresponding β spin orbitals.

nominally the oxo levels), and above those the set of nominally 3d levels. We wish to draw attention to the enormous difference in the α-3σ* (α-3d_{z^2}) orbital energy in the two diagrams (ca. 3 eV), making the α-3σ* of the $(H_2O)_5FeO^{2+}$ by far the stronger electron acceptor.

Obviously, the replacement of N donor ligands by O donor ligands causes a large stabilization of the α-3σ*. The triplet to quintet spin state change contributes to this effect, but is not solely responsible. Emptying the α-$d_{x^2-y^2}$, when it is being pushed up too high by strong equatorial ligands like NH_3 groups, and occupying the β-d_{xy}, reduces the number of unpaired spins from 4 in the quintet $(H_2O)_5FeO^{2+}$ to only 2 in the triplet $(NH_3)_5FeO^{2+}$. The stabilizing exchange field for the α spin levels then becomes much weaker. When the α-$d_{x^2-y^2}$ electron is flipped to β and put into β-d_{xy}, that is, spin paired with α-d_{xy} to form the $(d_{xy})^2$ pair, without changing the ligands, the net loss of stabilization of α-3σ* is about 1 eV, one-third of the total shift of about 3 eV displayed in Figure 1. The remainder of the shift comes from the stronger donation by the N lone pairs, both in terms of interaction strength (governed by Hamiltonian matrix element and fragment orbital energy difference) and in terms of charge effect.

It is clear that the relative importance of the α-3σ* as acceptor orbital (very important in the Fenton complex $(H_2O)_5FeO^{2+}$ compared to the β-2π* orbitals (more important with the N donor ligands) depends on the ligand environment.[10,17−19] We note that the balance between the α-σ* FMO channel and the β-π* channel[19] for oxidation reactions also depends on the metal used, as has been demonstrated in the series of complexes $(H_2O)_5MO^{2+}$ (M = V−Ni).[20] It is obvious that the energy of the α-3σ* can be further lowered if the *trans* axial ligand is very weak or absent. Therefore the design principles for a highly active FeO^{2+} hydroxylation catalyst are as follows:[16] (a) equatorial ligands should be weak donors, for example, preferably not the N lone pair donors used widely in the biomimetic analogues, but rather the weaker oxygen lone pair donors; (b) a weak or preferably absent *trans* axial donor. Very recently Que and co-workers have synthesized an interesting modification of the generally used nitrogen donor based pentacoordinate ligands like TMC, which have an equatorial square of four N donors and a *trans* axial N donor.[21] By replacing it with TMG_3tren (a tetradentate ligand that coordinates the iron with three equatorial and one *trans* axial N lone pair), the difference in the destabilizations of the equatorial $d_{x^2-y^2}$ and d_{xy} is lifted, these orbitals becoming degenerate by symmetry. In this ligand environment it is easier for the FeO^{2+} unit to retain the high-spin configuration, which indeed it does. On the other hand, the ligand environment still consists of all strong N donors, including a strong *trans* axial donor, destabilizing the α-d_{z^2}. Indeed, the reactivity of this newly synthesized complex was not extreme. We note that biological systems

(17) Neidig, M. N.; Decker, A.; Choroba, O. W.; Huang, F.; Kavana, M.; Moran, G. R.; Spencer, J. B.; Solomon, E. I. *Proc. Natl. Acad. Sci. U.S.A.* **2006**, *103*, 12966.
(18) Louwerse, M. J.; Baerends, E. J. *Phys. Chem. Chem. Phys.* **2007**, *9*, 156.
(19) Decker, A.; Rohde, J.-U.; Klinker, E. J.; Wong, S. D.; Que, L.; Solomon, E. I. *J. Am. Chem. Soc.* **2007**, *129*, 15983.
(20) Michel, C.; Baerends, E. J. *Inorg. Chem.* **2009**, *48*, 3628.
(21) England, J.; Martino, M.; Farquhar, E. R.; Frisch, J. R.; Bominaar, E. L.; Münck, E.; Que, L., Jr. *Angew. Chem., Int. Ed.* **2009**, *48*, 3622.

like TauD and MMO are characterized by more oxygen than nitrogen donor ligands.

On the basis of the design principles put forward above, EDTA has been proposed as a ligand that should be very effective, combining equatorial oxygen donors with a weak *trans* axial donor (two off-axis N lone pairs at large distance).[16] In the present contribution we will propose that the catalytic activity of the well-known α-oxygen in Fe-ZSM-5 can be considered from the same point of view: it possibly owes its high oxidative power to the presence of a FeO^{2+} unit in exactly the favorable ligand environment of equatorial oxygen ligands and absence of a *trans* axial donor.

Iron exchanged ZSM-5 has been shown to be an active catalyst for many reactions, a very interesting example being the decomposition of N_2O. This process has been suggested to proceed via oxidation of Fe^{2+} to Fe^{3+}, forming active oxygen species called by Panov and co-workers atomic α-oxygen.[22,23] This α-oxygen species is capable of selectively and quantitatively converting benzene to phenol at ambient temperature,[24,25] similar to the active oxygen of monooxygenases (MMOs), for which the hydroxylation of aromatics is a typical reaction.[26] The α-oxygens in Fe-ZSM-5 zeolites react at room temperature even with methane, the most inert organic molecule, giving quantitative yield of methanol,[27] thus challenging the reactivity of the active oxygen of methane monooxygenases (MMO).[28−33] Dubkov et al.[34] studied the kinetic isotope effect (KIE = k_H/k_D) for the methane and benzene oxidations by α-oxygen and found high KIE values (1.9−5.5, depending on the reaction temperature) for methane oxidation and no isotopic effect for benzene oxidation. This means that, similar to the MMO case, methane oxidation by α-oxygen involves the cleavage of the C−H bond as the rate-limiting step. The oxidation of benzene proceeds somewhat differently. Understandably, benzene is attacked by the electrophilic FeO^{2+} at its π electron cloud, as has been found for benzene hydroxylation with biomimetic non-heme FeO^{2+} complexes[35] and with a zeolite cluster with FeO^{2+}.[36] Therefore, in many respects, α-oxygen in Fe-ZSM-5 zeolites exhibits an exciting analogy to the active oxygen in MMO: in both cases oxygen species coordinated to Fe complexes show very high reactivity and produce the same products via the same type of mechanism. For this reason such materials were called "mineral enzymes" or "zeozymes".[37,38]

The location and nuclearity of α-sites (an α-site is defined as an iron entity able to adsorb one atom of α-oxygen), have been extensively debated.[38] It is by now widely accepted that the α-sites are located inside the channels of the zeolite matrix.[39−42] The nuclearity of the α-sites is less clear, although significant evidence has been given that they are monatomic and in a paired arrangement, with each of the Fe ions in the binuclear structure being capable of generating α-oxygen species independently.[23] Although the oxygen species involved in the C−H bond activation have not been identified experimentally, $[FeO]^+$, $[Fe(O)_2]^+$, $[OFeO]^+$, and $[FeO]^{2+}$ species have been proposed as the catalytically active centers on the basis of quantum chemical calculations.[43−48] Depending on the ironoxo species assumed as the catalytic active center, different C−H bond activation mechanisms have been theoretically proposed.

$[FeO]^+$ with a d^5 Fe(III) has been assumed as the active catalytic center by Yoshizawa et al.[43] We wish to stress that the $[FeO]^+$ would have to accommodate the extra electron it possesses compared to $[FeO]^{2+}$ in the α-d_{z^2} orbital, which we view[16,18] as the prime acceptor orbital of this moiety, responsible for its extreme electrophilicity and high activity in C−H functionalization. This will lead to much higher barriers than expected for $[FeO]^{2+}$. The authors of ref 43 studied the reaction pathways and the energetics for the direct hydroxylation of methane and of benzene over $[FeO]^+$ in the Fe-ZSM-5 zeolite surface. The barrier height computed for the second transition state in the two-step process, TS2, is quite high (41.6 and 31.1 kcal/mol in the case of methane and benzene, respectively). The proposed mechanism does not account for the high KIE values measured for methane oxidation by zeolite α-oxygen.[34] A d^5 Fe(III) iron center with occupied α-d_{z^2} is also advocated in the theoretical work by Malykhin et al.,[48] who propose an electronic configuration $[Fe(III)O^{\cdot -}]^{2+}$. These authors note however that in their calculations on the model system $FeO(OH)_2$, the lowest energy configuration at the minimum energy geometry does have a d^4 Fe(IV) iron center, that is, empty α-d_{z^2}. Important recent experimental evidence, based on resonant inelastic

(22) Panov, G. I.; Uriarte, A. K.; Rodkin, M. A.; Sobolev, V. I. *Catal. Today* **1998**, *41*, 365.
(23) Dubkov, K. A.; Ovanesyan, N. S.; Shteinman, A. A.; Starokon, E. V.; Panov, G. I. *J. Catal.* **2002**, *207*, 341.
(24) Sobolev, V. I.; Kharitonov, A. S.; Paukshtis, Y. A.; Panov, G. I. *J. Mol. Catal.* **1993**, *84*, 117.
(25) Panov, G. I.; Sobolev, V. I.; Dubkov, K. A.; Parmon, V. N.; Ovanesyan, N. S.; Shilov, A. E.; Shteinman, A. A. *React. Kinet. Catal. Lett.* **1997**, *61*, 251.
(26) Shilov, A. E. *Metal Complexes in Biomimetic Chemical Reactions*; CRC Press: New York, 1997.
(27) Panov, G. I.; Sobolev, V. I.; Dubkov, K. A.; Kharitonov, A. S. *Stud. Surf. Sci. Catal.* **1996**, *101*, 493.
(28) Dewitt, J. G.; Bentsen, J. G.; Rosenzweig, A. C.; Hedman, B.; Green, J.; Pilkington, S.; Papaefthymion, G. C.; Dalton, H.; Hodgson, K. O.; Lippard, S. J. *J. Am. Chem. Soc.* **1991**, *113*, 9219.
(29) Shteinman, A. A. *Russ. Chem. Bull.* **2001**, *50*, 1795.
(30) Que, L. *Pure Appl. Chem.* **1998**, *70*, 947.
(31) Kopp, D. A.; Lippard, S. J. *Curr. Opin. Chem. Biol.* **2002**, *6*, 568.
(32) Siegbahn, P. E. M.; Crabtree, R. H.; Nordlund, P. *J. Biol. Inorg. Chem.* **1998**, *3*, 314.
(33) Lieberman, R. L.; Rosenzweig, A. C. *Nature* **2005**, *34*, 177.
(34) Dubkov, K. A.; Sobolev, V. I.; Talsi, E. P.; Rodkin, M. A.; Watkins, N. H.; Shteinman, A. A.; Panov, G. I. *J. Mol. Catal.* **1997**, *123*, 155.
(35) de Visser, S. P.; Oh, K.; Han, A.-R.; Nam, W. *Inorg. Chem.* **2007**, *46*, 4632.
(36) Fellah, M. F.; van Santen, R. A.; Onal, I. *J. Phys. Chem. C* **2009**, *113*, 15307.
(37) Parton, R.; De Vos, D.; Jakobs, P. A. In *Zeolite Micropores Solids: Synthesis, Structure and Reactivity*; Derouane, E. G., Ed.; Kluwer: The Netherlands, 1992; p 555.
(38) Panov, G. I. *CATTECH* **2000**, *4*, 18.
(39) Ribera, A.; Arends, I. W. C. E.; de Vries, S.; Perez-Ramires, J.; Sheldon, R. A. *J. Catal.* **2000**, *195*, 287.
(40) Pirutko, L. W.; Parenago, O. O.; Lunina, E. V.; Kharitonov, A. S.; Okkel, L. G.; Panov, G. I. *React. Kinet. Catal. Lett.* **1994**, *52*, 275.
(41) Panov, G. I.; Kharitonov, A. S.; Fenelonov, V. B.; Voskresenskaya, T. P.; Rudina, N. A.; Molchanov, V. V.; Plyasova, M. L. *Zeolites* **1995**, *15*, 253.
(42) Pirutko, L. W.; Dubkov, K. A.; Solovjeva, L. P.; Panov, G. I. *React. Kinet. Catal. Lett.* **1996**, *58*, 105.
(43) Yoshizawa, A. L.; Shiota, Y.; Yumura, T.; Yamabe, T. *J. Phys. Chem. B* **2000**, *104*, 734.
(44) Kachurovskaya, N. A.; Zhidomirov, G. M.; Hensen, E. J. M.; van Santen, R. A. *Catal. Lett.* **2003**, *86*, 25.
(45) Kachurovskaya, N. A.; Zhidomirov, G. M.; van Santen, R. A. *J. Phys. Chem. B* **2004**, *108*, 5944.
(46) Ryder, J. A.; Chakraborty, A. K.; Bell, A. T. *J. Catal.* **2003**, *220*, 84.
(47) Liang, W.-Z.; Bell, A. T.; Head-Gordon, M.; Chakraborty, A. K. *J. Phys. Chem. B* **2004**, *108*, 4362.
(48) Malykhin, S.; Zilberberg, I.; Zhidomirov, G. M. *Chem. Phys. Lett.* **2005**, *414*, 434.

X-ray scattering, has been put forward that supports d^5 Fe(III) rather than d^4 Fe(IV) in the zeolite.[49,50] In theoretical work on the decomposition of N_2O over Fe exchanged zeolite Bell et al. have assumed a FeO^+ active center to start with, which they showed may lead to the peroxo species $[FeO_2]^+$ and the dioxo species $[OFeO]^+$ as active sites for methane hydroxylation.[47]

$[FeO]^{2+}$ has long been known to be the active center in heme enzymes such as cytochrome P450[1,2] and has been suggested to be also responsible for the catalytic activity of Fe-ZSM-5 zeolites.[22,51] $[FeO]^{2+}$ with a d^4 Fe(IV) iron center has been considered as the active catalytic species by Kachurovskaya et al.[44,45] and Fellah et al.[36] in their DFT studies of the benzene-to-phenol oxidation reaction on iron exchanged zeolites. These authors proposed a reaction path for the benzene oxidation that is consistent with the experimental evidence for the absence of the kinetic H/D isotope effect in phenol formation.

In this work we study the methane hydroxylation reaction catalyzed by the ferryl ion $[FeO]^{2+}$ in the active center on Fe-ZSM-5 zeolites. Specifically, we want to investigate whether the ligand environments offered by plausible cation exchange sites of the ZSM-5 zeolite conform to the requirements put forward above for high activity of $[FeO]^{2+}$ as a hydroxylation catalyst. We will come to the conclusion that the design principles for optimal activity of $[FeO]^{2+}$, which are weak equatorial donor ligands, and a very weak or absent *trans* axial donor, are perfectly met by the ligand environments for $[FeO]^{2+}$ in this case. This connects the Fe-ZSM-5 zeolite catalyst for methane hydroxylation immediately with the active biological systems for this reaction, such as TauD and MMO. The rebound mechanism proposed by Groves[52,53] and generally accepted for C−H oxidation by metal oxo complexes also applies in this case.

Methods

The calculations were done with ADF (Amsterdam Density Functional)[54−56] as well as with TURBOMOLE V6.0[57,58] packages. Two GGA (Generalized Gradient Approximation) exchange-correlation functionals were employed, BP86[59,60] and OPBE.[61,62] The use of both these functionals is needed to provide reliable prediction of both the geometries and spin-state energetics of the reaction intermediates. The BP86 functional provides quite accurate geometries and bond energies of first-row transition metal complexes,[63−65] but fails in describing close-lying spin states, in particular in iron complexes.[64,66,67] On the other hand, the OPBE functional has been shown to yield correct spin state relative stabilities for various inorganic and organometallic iron complexes,[68−71] but fails in describing weak bonds, including hydrogen bonds and $\pi-\pi$ stacking interactions.[64,66,67,72] For sake of comparison with previous studies on the C−H activation reactivity of Fe-ZSM-5 zeolites, the calculations on the catalytic active iron(IV)-oxo species in the high-spin ($S = 2$) and low-spin ($S = 1$) states were also performed at the B3LYP[59,73,74] level of theory, using TURBOMOLE. All calculations were performed in the gas-phase using the spin-unrestricted approach. The BP86 and OPBE ADF calculations included relativistic effects through the Zero-Order Regular Approximation (ZORA) and made use of a basis set of Slater type orbitals of TZ2P quality for all atomic species. The BP86 and B3LYP TURBOMOLE calculations were performed with the recent triple-ζ all-polarizable basis set, def2-TZVP,[75] which provides a balanced description of all elements of the periodic table. In the BP86 TURBOMOLE calculations, the resolution of the identity (density fitting) approach was used to save computer time.[76]

Transition states were found by first performing a potential energy scan along the pertinent reaction coordinate. The maximum energy structures were then taken as a guess for the transition state search. Frequency calculations were performed to characterize local minima and transition states. The transition states described here had one imaginary frequency for the correct mode, whereas all local minima had real frequencies only. Zero-point energies (ZPE) corrections were obtained from the frequency calculations and are included in the reaction energies and activation energies throughout.

The kinetic isotope effect (KIE) of replacing hydrogen by deuterium atoms in the methane was estimated using the semiclassical model based on Eyring's eq 1.

$$k_H/k_D = \exp[-(\Delta G^{\ddagger}_H - \Delta G^{\ddagger}_D)/RT] \quad (1)$$

As the KIEs originate, in this framework, from isotopic ZPE differences between the reactant (R) and transition state, the thermal factors playing a very minor role, the $(\Delta G^{\ddagger}_H - \Delta G^{\ddagger}_D)$ term was approximated by the $(ZPE^{\ddagger}_H - ZPE^{R}_H - ZPE^{\ddagger}_D + ZPE^{R}_D)$ term.

Model System. In our model of the "α-oxygen" species, ZFeO (Z = zeolite), the zeolite is represented by the dianionic cluster previously used by Kachurovskaya et al.[44] This cluster is

(49) Pirngruber, G. D.; Grunwaldt, J. D.; van Bokhoven, J. A.; Kalytta, A.; Reller, A.; Safonova, O. V.; Glatzel, P. *J. Phys. Chem. B* **2006**, *110*, 18104.
(50) Pirngruber, G. D.; Grunwaldt, J. D.; Roy, P. K.; van Bokhoven, J. A.; Safonova, O. V.; Glatzel, P. *Catal. Today* **2007**, *126*, 127.
(51) Kiwi-Minsker, L.; Bulushev, D. A.; Renken, A. *J. Catal.* **2003**, *219*, 273.
(52) Groves, J. T.; McClusky, G. A. *J. Am. Chem. Soc.* **1976**, *98*, 859.
(53) Groves, J. T. *J. Chem. Educ.* **1985**, *62*, 928.
(54) Fonseca Guerra, C.; Snijders, J. G.; te Velde, G.; Baerends, E. J. *Theor. Chem. Acc.* **1998**, *99*, 391.
(55) *ADF2008.01*; SCM, Theoretical Chemistry, Vrije Universiteit Amsterdam: The Netherlands; http://www.scm.com.
(56) te Velde, G.; Bickelhaupt, F. M.; Baerends, E. J.; Fonseca Guerra, C.; van Gisbergen, S. J. A.; Snijders, J. G.; Ziegler, T. *J. Comput. Chem.* **2001**, *22*, 931.
(57) *TURBOMOLE* V6.0 2009; a development of University of Karlsruhe and Forschungzentrum Karlsruhe GmbH, 1989−2007; TURBOMOLE GmbH: Karlsruhe, Germany, 2007; available from http://www.turbomole.com.
(58) Ahlrichs, R.; Bär, M.; Häser, M.; Horn, H.; Kölmel, C. *Chem. Phys. Lett.* **1989**, *162*, 165.
(59) Becke, A. *Phys. Rev. A* **1988**, *38*, 3098.
(60) Perdew, J. P. *Phys. Rev. B* **1986**, *33*, 8822.
(61) Cohen, A. J.; Handy, N. C. *Mol. Phys.* **2001**, *99*, 607.
(62) Perdew, J. P.; Burke, K.; Ernzerhof, M. *Phys. Rev. Lett.* **1997**, *78*, 1396.
(63) Jensen, K. P.; Roos, B. O.; Ryde, U. *J. Chem. Phys.* **2007**, *126*, 014103.
(64) Neese, F. *J. Biol. Inorg. Chem.* **2006**, *11*, 702.
(65) Berry, J. F.; DeBeer, G. S.; Neese, F. *Phys. Chem. Chem. Phys.* **2008**, *10*, 4361.
(66) Ghosh, A. *J. Biol. Inorg. Chem.* **2006**, *11*, 712.
(67) Radón, M.; Pierloot, K. *J. Phys. Chem. A* **2008**, *112*, 11824.
(68) Fouqueau, A.; Mer, S.; Casida, M. E.; Daku, L. M. L.; Hauser, A.; Mineva, T.; Neese, F. *J. Chem. Phys.* **2004**, *120*, 9473.
(69) Fouqueau, A.; Casida, M. E.; Lawson, L. M.; Hauser, A.; Neese, F. *J. Chem. Phys.* **2005**, *122*, 044110.
(70) Swart, M.; Groenhof, A. R.; Ehlers, A. W.; Lammertsma, K. *J. Phys. Chem. A* **2004**, *108*, 5479.
(71) Conradie, J.; Quarless, D.; Hsu, H.-F.; Harrop, T.; Lippard, S. J.; Koch, S.; Ghosh, A. *J. Am. Chem. Soc.* **2007**, *129*, 10446.
(72) Swart, M.; Solà, M.; Bickelhaupt, F. M. *J. Chem. Phys.* **2009**, *131*, 094103.
(73) Becke, A. D. *J. Chem. Phys.* **1993**, *98*, 5648.
(74) Lee, C.; Yang, W.; Parr, R. G. *Phys. Rev. B* **1988**, *37*, 785.
(75) Weigend, F.; Ahlrichs, R. *Phys. Chem. Chem. Phys.* **2005**, *7*, 3297.
(76) Eichkorn, K.; Treutler, O.; Häser, M.; Ahlrichs, R. *Chem. Phys. Lett.* **1995**, *240*, 283.

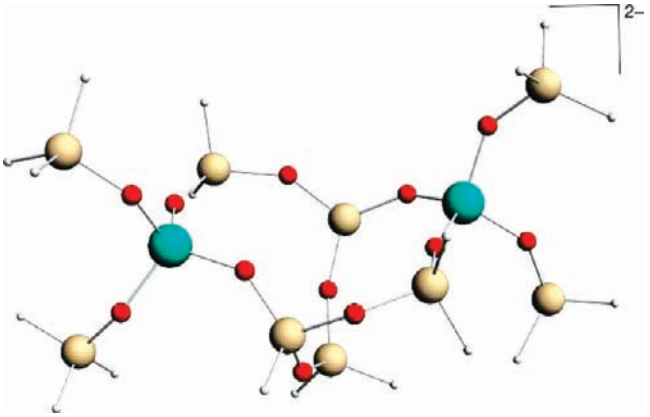

Figure 2. Zeolite cluster model. Color code: aluminum (green), silicon (sand), oxygen (red), hydrogen (white).

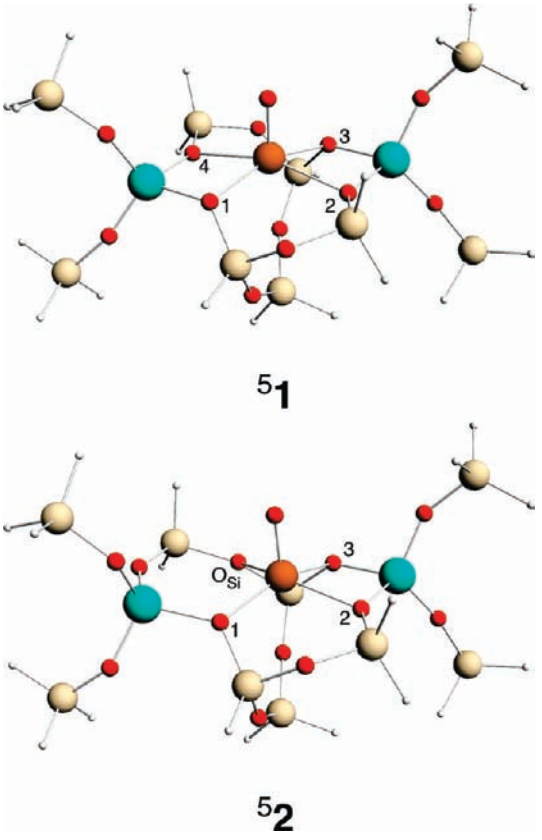

Figure 3. BP86/ZORA/TZ2P optimized structures of the **1** and **2** isomers of ZFeO in the quintet spin state. Color code: iron (rust brown), aluminum, silicon, oxygen, and hydrogen as in Figure 2.

constructed from two intersecting five-membered zeolite rings. Two distant Si atoms were replaced by Al atoms, so that in the surface a six-membered ring of two Al's and four O's is formed (Figure 2). The initial coordinates of the cluster were taken from crystallographic data for the α-position of MFI.[77] In the six-membered ring, hydrogen atoms were used to saturate broken Si−O bonds, while Al atoms were saturated by $-OSiH_3$ groups. The positions of the boundary hydrogen atoms were optimized keeping frozen the positions of all the other atoms and with saving the crystal structure directions of the boundary bonds. The doubly negative charge of the two Al-substituted T-sites is compensated by the iron oxo species, $[FeO]^{2+}$, placed in the

(77) Chao, K.; Lin, J.; Wang, Y.; Lee, G. H. *Zeolites* **1986**, *6*, 35.

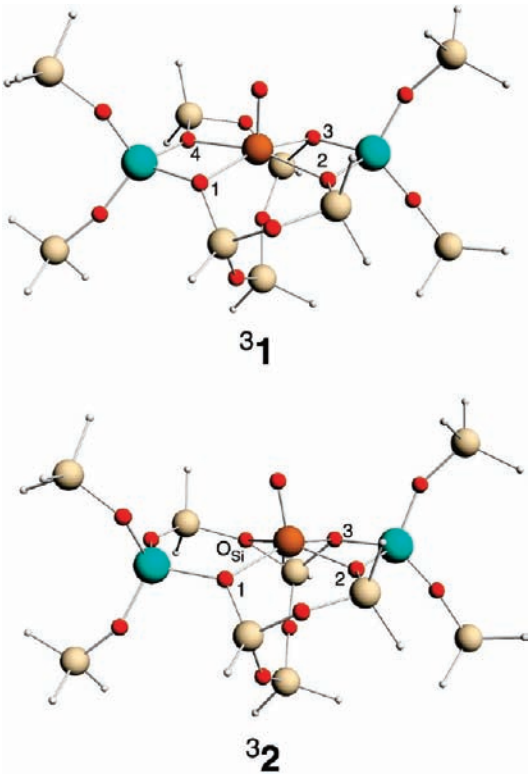

Figure 4. BP86/ZORA/TZ2P optimized structures of the **1** and **2** isomers of ZFeO in the triplet spin state. Color code as in Figure 3.

cavity of the zeolite six-membered ring, as shown in Figures 2 and 3. The structure of the ZFeO cluster as well as of the species involved in the methane hydroxylation reaction were optimized without constraints except for the positions of the boundary hydrogen atoms at the $-OSiH_3$ groups, which were kept fixed. For the ZFeO cluster the $S = 0$, 1, 2, and 3 spin states were considered. The $S = 2$ spin state was found to be the ground state, with the $S = 1$ being the next higher spin state (vide infra). The $S = 0$ and $S = 3$ spin states were found much higher in energy than the quintet state; therefore we did not pursue these spin surfaces further, and the complete reaction profile for methane hydroxylation was studied only on the triplet and quintet spin state surfaces.

Results and Discussion

Molecular and Electronic Structure of the Fe-ZSM-5 "α-oxygen" Model. Two coordination geometries of the iron atom to the oxygen atoms of the zeolite ring were considered, **1** and **2**. In **1** the iron coordinates to the four oxygen atoms bonded to the Al atoms, as in the ZFeO cluster model by Kachurovskaya et al.[44] In **2** the iron atom coordinates to three oxygen atoms bonded to the Al atoms and an oxygen atom bonded only to Si atoms. This type of coordination has been reported for the zinc ion in a six-membered zeolite ring similar to that of our cluster model.[78]

The $S = 2$ and $S = 1$ optimized structures of **1** and **2** are displayed in Figures 3 and 4, respectively.

The important geometrical parameters, relative energies, Mulliken spin and charge populations computed at different levels of theory are reported in Tables 1 and 2.

(78) Shubin, A. A.; Zhidomirov, G. M.; Yakovlev, A. L.; van Santen, R. A. *J. Phys. Chem. B* **2001**, *105*, 4928.

Table 1. Geometrical Parameters (in Å), Spin Densities (ζ), Charges (q), and Relative Energies (in kcal mol^{-1}) of the $S = 2$ Structures **1** and **2** as a Model for α-oxygen in Fe-ZSM-5 Zeolites

	1				**2**			
$S = 2$	BP86[a]	BP86[b]	OPBE[a]	B3LYP[b]	BP86[a]	BP86[b]	OPBE[a]	B3LYP[b]
Fe−O_{ax}	1.603	1.605	1.581	1.589	1.607	1.609	1.585	1.590
Fe−O_1	1.994	2.015	1.985	2.020	1.991	2.016	1.995	2.021
Fe−O_2	2.184	2.181	2.206	2.172	2.085	2.090	2.068	2.083
Fe−O_3	2.050	2.081	2.043	2.080	2.158	2.179	2.134	2.145
Fe−O_4	2.251	2.247	2.290	2.253				
Fe−O_{Si}					2.277	2.262	2.343	2.270
Δ_{Fe}[c]	0.41	0.41	0.32	0.46	0.53	0.55	0.44	0.56
ΔE[d]	+ 0.5	0.0	+ 0.7	0.0	+ 0.0	+ 0.3	0.0	+ 0.01
ζ_{Fe}	3.07	3.06	3.15	3.30	3.13	3.08	3.21	3.31
$\zeta_{O_{ax}}$	0.62	0.64	0.61	0.43	0.62	0.63	0.60	0.41
q_{Fe}	+ 1.03	+ 0.70	+ 1.07	+ 0.90	+ 1.03	+ 0.78	+ 1.08	+ 0.97
$q_{O_{ax}}$	−0.36	−0.31	−0.39	−0.34	−0.38	−0.32	−0.41	−0.33

[a] ADF (ZORA/TZ2P). [b] Turbomole (def2-TZVP). [c] Displacement of the iron atom from the plane defined by the four equatorial oxygen atoms. [d] Energies include ZPE correction.

Table 2. Geometrical Parameters (in Å), Spin Densities (ζ), Charges (q), and Relative Energies (in kcal mol^{-1}) of the $S = 1$ Structures **1** and **2** as a Model for α-oxygen in Fe-ZSM-5 Zeolites

	1				**2**			
$S = 1$	BP86[a]	BP86[b]	OPBE[a]	B3LYP[b]	BP86[a]	BP86[b]	OPBE[a]	B3LYP[b]
Fe−O_{ax}	1.603	1.605	1.578	1.584	1.574	1.574	1.550	1.564
Fe−O_1	1.965	1.972	1.951	1.973	2.058	2.100	2.071	2.094
Fe−O_2	2.040	2.046	2.025	2.053	1.929	1.943	1.892	1.941
Fe−O_3	2.030	2.045	2.014	2.034	2.006	2.020	1.958	1.981
Fe−O_4	2.107	2.114	2.130	2.134				
Fe−O_{Si}					2.405	2.376	2.487	2.332
Δ_{Fe}[c]	0.30	0.29	0.23	0.33	0.50	0.53	0.43	0.50
ΔE[d]	0.0	0.0	0.0	0.0	+ 4.6	+ 5.1	+ 2.7	+ 6.6
ζ_{Fe}	1.24	1.24	1.28	1.18	1.54	1.59	1.60	1.33
$\zeta_{O_{ax}}$	0.79	0.81	0.78	0.85	0.49	0.49	0.46	0.67
q_{Fe}	+ 0.94	+ 0.52	+ 0.95	+ 0.72	+ 0.97	+ 0.69	+ 1.01	+ 0.85
$q_{O_{ax}}$	−0.37	−0.30	−0.39	−0.32	−0.36	−0.32	−0.38	−0.33
ΔE(T−Q)[d,e]	+ 2.7	+ 2.5	+ 11.7	+ 12.1	+ 7.7	+ 7.3	+ 15.2	+ 18.7

[a] ADF (ZORA/TZ2P). [b] TURBOMOLE (def2-TZVP). [c] Displacement of the iron atom from the plane defined by the four equatorial oxygen atoms. [d] Energies include ZPE correction. [e] Energy difference between the triplet and quintet spin states.

Table 2 also reports for each structure the energy difference between the triplet and quintet spin states, ΔE (T−Q). Inspection of the ΔE (T−Q) values reveals that the quintet spin state is invariably lower in energy than the triplet state for both structures, particularly for **2**.

The high-spin (quintet) state is favored by the rather weak σ-donor ability of the O-based equatorial ligands.[16,79] The energy gap to the first excited spin state, the $S = 1$ state, depends on the density functional used, being at the BP86 level significantly smaller than at the OPBE and B3LYP level.

Several studies have established that while pure functionals, like BP86, overly stabilize low-spin states, the hybrid functional B3LYP in general favors high spin states.[19,80−83] Thus, the actual energy difference between the $S = 1$ and $S = 2$ states likely lies somewhere in between the calculated values. The OPBE functional has been found to perform relatively well for the singlet−triplet splitting in iron compounds.[70] It is worth noting that the triplet-quintet splitting is at the OPBE level only slightly smaller than at the B3LYP level, which is in line with recent results by Hirao et al.[15] on various oxo-iron complexes.

Quintet Species ^{5}1 and ^{5}2. According to the calculated energies, the **1** and **2** isomers are nearly degenerate in their quintet ground spin state. Thus, ^{5}**1** and ^{5}**2** are both plausible models for the catalytic site. In the first excited spin state the energies of the **1** and **2** structures lie within 3−7 kcal/mol, with the more symmetric isomer **1** being the preferred one, particularly at the B3LYP and BP86 level of theory. As the crystal structure directions of the boundary bonds are preserved in our cluster model, the structural variability observed for ZFeO is not an artifact of the chosen model. Rather, it is indicative of the inherent flexibility of the six-membered zeolite ring. This flexibility is expected to be enhanced in the real system

(79) Neese, F. *J. Inorg. Biochem.* **2006**, *100*, 716.
(80) Paulsen, H.; Duelund, L.; Winkler, H.; Toflund, H.; Trautwein, H. X. *Inorg. Chem.* **2001**, *40*, 2201.
(81) Salomon, O.; Reiher, M.; Hess, B. A. *J. Chem. Phys.* **2002**, *117*, 4729.
(82) Reiher, M. *Inorg. Chem.* **2002**, *41*, 6928.
(83) Vargas, A.; Zerara, M.; Krausz, E.; Hauser, A.; Daku, L. M. L. *J. Chem. Theory Comput.* **2006**, *2*, 1342.

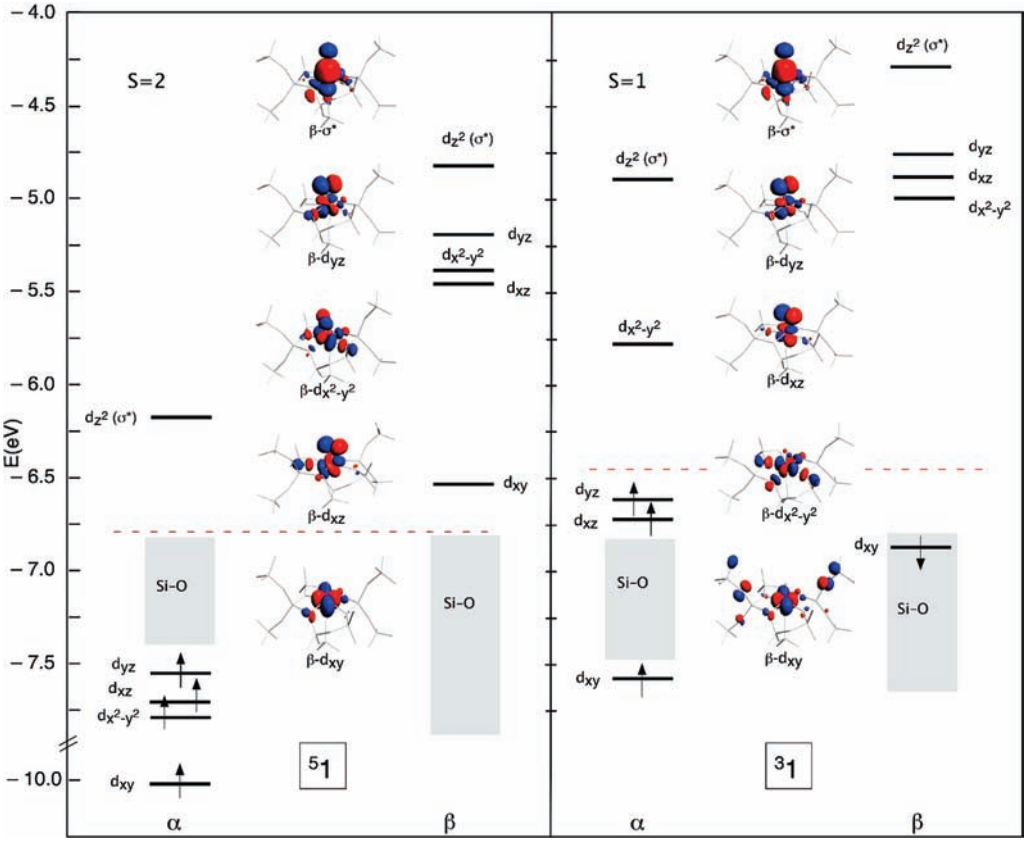

Figure 5. Energy level diagram and molecular orbitals of ^{3,5}**1** obtained from DFT/ZORA/BP86/TZ2P calculations.

where the boundary Si−H bonds are replaced by the more flexible Si−O bonds.

Focusing on the geometrical details of **1** and **2** in the quintet ground spin state (Figure 3), both isomers show a Fe−O_{ax} distance of about 1.6 Å (see Table 1), which is typical for iron(IV)-oxo complexes[7,84] with the iron lying 0.3−0.6 Å above the plane of the equatorial oxygen atoms. As can be inferred from the data in Table 1, the spin population at the iron and oxo-ligand is scarcely influenced by the geometrical changes in the equatorial coordination and compares well to that computed for other $S = 2$ iron(IV)-oxo complexes.[85,86] In the more symmetric isomer **1**, two *trans* Fe−O bonds, Fe−O_1 and Fe−O_3, are significantly shorter than the other two, Fe−O_2 and Fe−O_4. In the less symmetric isomer ^{5}**2** there are also two short and two long Fe−O bonds, the *cis* Fe−O_1 and Fe−O_2, and the *cis* Fe−O_3 and Fe−O_{Si} bonds, respectively.

Complexes **1** and **2** in the quintet ground spin state have qualitatively the same electronic structure and bonding scheme. They retain the distinctive electronic structure features of most $S = 2$ iron(IV)-oxo complexes studied to date, as inferred from Figures 5 and 6 where the spin unrestricted energy level diagrams and relevant molecular orbitals of ^{3,5}**1** and ^{3,5}**2** are displayed.

The Fe(IV)=O ($S = 2$) is a d^4 system with a $(d_{xy})^1(d_{x^2-y^2})^1(d_{xz})^1(d_{yz})^1$ ground configuration. The Fe−O bond is formed by a σ interaction between the (nominally occupied) O-$2p_z$ orbital and the (nominally unoccupied) Fe-d_{z^2} orbital, and a π interaction between the (nominally occupied) O-$2p_{x,y}$ and the (nominally half occupied) Fe-$d_{xz,yz}$ orbitals, cf. the 1σ and $1\pi_{x,y}$ doubly occupied orbitals in Figure 1. In the diagrams of Figures 5 and 6 only the antibonding orbitals (which are nominally the d orbitals) of σ and π symmetry are reported. The oxygen contribution to these orbitals ranges from 36% to 46%.

Of the Fe-d_δ orbitals, the half occupied d_{xy} is substantially a nonbonding orbital, whereas the $d_{x^2-y^2}$ with lobes along the axes is pushed up by antibonding interaction with the σ lone pairs of the equatorial oxygen ligands[10] (but much less so than with N donor ligands[16]). The interaction with the equatorial ligands is stronger in **1** than in **2**, as indicated by the energies of the antibonding $d_{x^2-y^2}$, the α and β components of which shift to higher energy by 0.25 and 0.30 eV, respectively. This is consistent with two of the equatorial Fe−O bonds being in the isomer **1** significantly shorter than in **2**. The stronger interaction of the zeolite ring with the iron center in **1**, is not reflected, however, in an increased charge donation to the iron, as the iron charge decreases only marginally on going from **2** to **1** (see Table 1). It is clear from the level schemes of Figures 5 and 6 that in both isomers the lowest acceptor molecular orbital, that is, the one that can accept density from the substrate C−H bond is the α component of the d_{z^2} (σ^*). The surplus of α electrons creates a strongly stabilizing exchange potential pulling all α levels, including the d_{z^2} (σ^*), very much down compared to the corresponding β levels. Notably, the α-d_{z^2} (σ^*) is in **2**

(84) Riggs-Gerlasco, P. J.; Price, J. C.; Gruyer, R. B.; Brehm, J. H.; Bart, E. W.; Bollinger, J. M., Jr.; Krebs, C. *J. Am. Chem. Soc.* **2004**, *126*, 8108.
(85) Sinnecker, S. S. N.; Barr, E. W.; Ye, S.; Bollinger, J. M., Jr.; Neese, F.; Krebs, C. *J. Am. Chem. Soc.* **2007**, *129*, 6168.
(86) Decker, A.; Solomon, E. I. *Angew. Chem., Int. Ed.* **2005**, *44*, 2252.

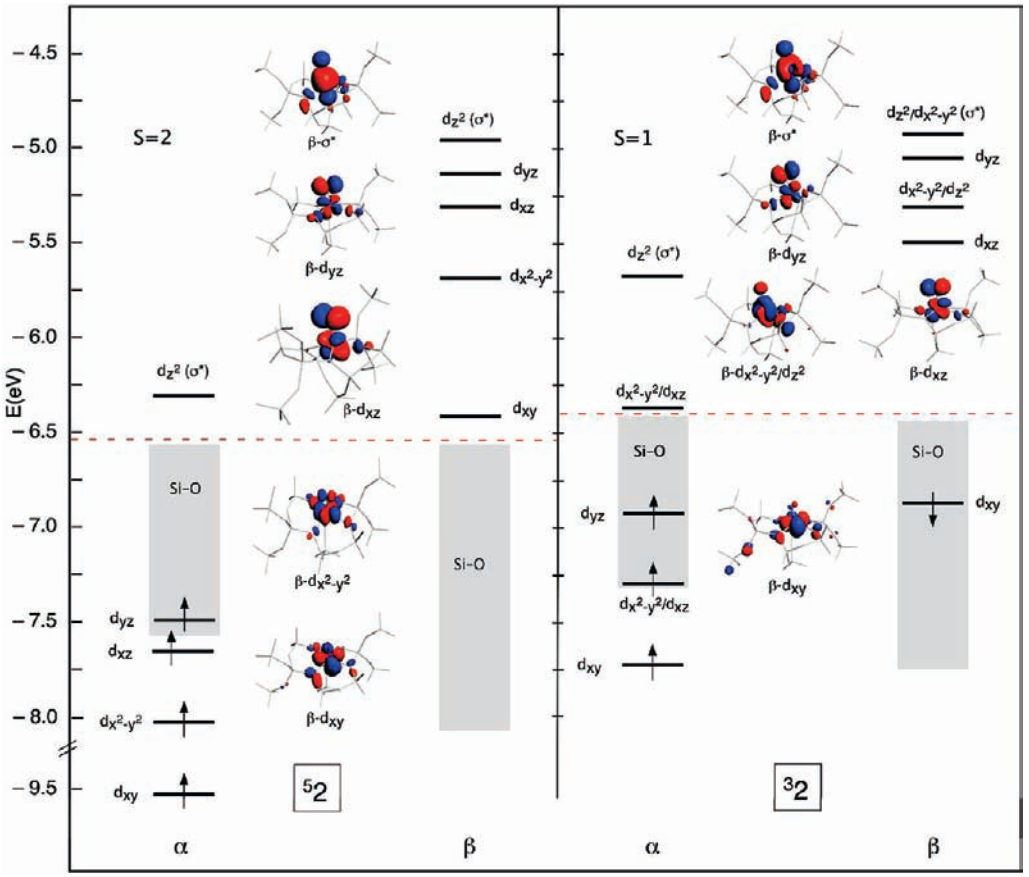

Figure 6. Energy level diagram and molecular orbitals of ^{3,5}**2** obtained from DFT/ZORA/BP86/TZ2P calculations.

Table 3. Energy Data (in kcal/mol) for the Methane Hydroxylation Reaction by ^{3,5}**1** and ^{5}**2**

	$\Delta E^{\ddagger}_{TS_H}$		$\Delta E_1{}^a$		$\Delta E^{\ddagger}_{TS_{reb}}$	$\Delta E_2{}^b$		ΔE^c	
	BP86[d]/BP86[e]	OPBE	BP86[d]/BP86[e]	OPBE	BP86[d]/BP86[e]	BP86[d]/BP86[e]	OPBE	BP86[d]/BP86[e]	OPBE
^{5}**1**	6.6/6.4	6.9	6.5/6.2	6.5	1.9/2.1	−41.2/−44.5	−38.7	−10.9/−13.8	−20.1
^{5}**2**	5.2/4.3	6.0	5.0/4.1	5.8	2.0/2.0	−39.9/−43.4	−37.6	−7.8/−12.1	−18.5
^{3}**1**	18.8/18.2	18.7	18.5/18.0	18.5	3.7/3.5	−34.4/−39.3	−35.0	−2.3/−4.8	−10.1

[a] $\Delta E_1 = E(\mathbf{I}) - E(\mathbf{R})$. [b] $\Delta E_2 = E(\mathbf{PC}) - E(\mathbf{I})$. [c] $\Delta E = E(\mathbf{P}) - E(\mathbf{R})$. [d] ADF (ZORA/TZ2P). [e] TURBOMOLE (def2-TZVP).

about 0.2 eV lower in energy than in **1**, on account of the reduced equatorial field in the former. As visible in the plots of the d_{z^2} (σ^*) in Figures 5 and 6, this orbital has some antibonding character with the equatorial oxygen lone pairs. The empty β-d_{xy}, which is actually lower in energy than the α-d_{z^2} (σ^*), in both ^{5}**1** and ^{5}**2**, and the empty β-$d_{x^2-y^2}$ will not play a role since they are not involved in the Fe−O_{ax} bonding and will be shielded from an incoming substrate molecule by the equatorial ligands. On the other hand, the β-$d_{xz,yz}$, which are also low-lying empty orbitals, are expected to be less important as acceptor orbitals than the α-d_{z^2} (σ^*), since they are more than 0.7 eV higher in energy. Nevertheless, involvement of these π orbitals, particularly the lowest one, the β-d_{xz}, is a distinct possibility.

Triplet Species ^{3}1 and ^{3}2. The bond lengths gathered in Table 3 for the $S = 1$ isomers show that, while the Fe−O_{ax} distance changes only marginally going from the quintet to the triplet state, the equatorial Fe−O bonds undergo significant changes. In **1** the equatorial Fe−O bonds experience a sensible contraction, specially the *trans* Fe−O_2 and Fe−O_4 bonds, to the result that in ^{3}**1** all four the equatorial Fe−O bonds have a comparable length. As can be inferred from the diagrams of Figure 2 the quintet and triplet electronic configurations differ by a spin-forbidden single ligand field transition from the α-$d_{x^2-y^2}$ to the β-d_{xy}. Since the former is strongly σ-antibonding with the equatorial ligands, but both are (nearly) perpendicular to the Fe−O_{ax} bond, it becomes evident why the Fe−O_{ax} bond does not change in going from the quintet to the triplet spin state, but the equatorial ligands bind much more strongly to the central iron in the triplet than in the quintet. In the isomer **2** two of the three equatorial Fe−O bonds involving the oxygen atoms bonded to the Al atoms, Fe−O_2 and Fe−O_3, shorten significantly, whereas the one involving the oxygen atom bonded only to Si atoms elongates. The lengthening of the Fe−O_{Si} bond and the shortening of the *trans* Fe−O_2 bond are particularly pronounced at the OPBE level. This is consistent with the well-known tendency of this functional to exaggerate the length of weak bonds *trans* to strong bonds.[66,67,79]

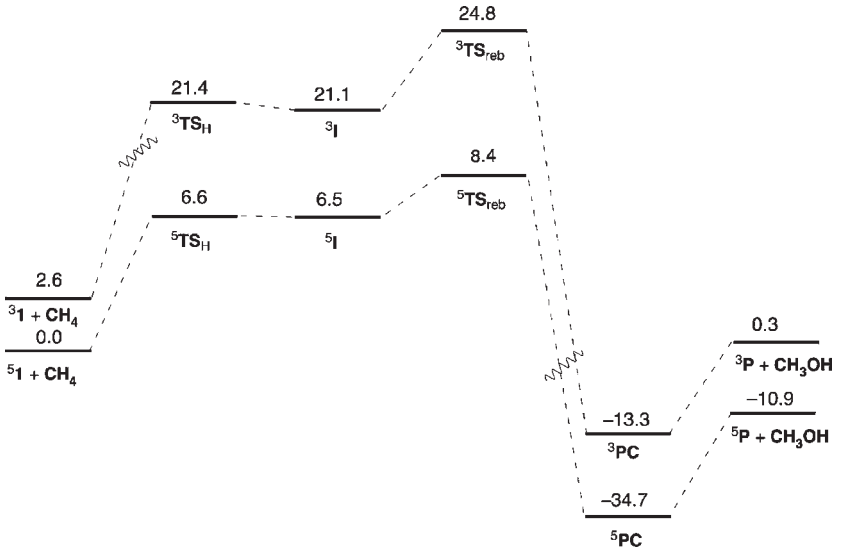

Figure 7. DFT/ZORA/BP86/TZ2P potential energy profiles for methane hydroxylation reaction by ^{3,5}**1**. Energies are in kcal/mol and include ZPE correction.

Scheme 1. Schematic Representation of the Rebound Mechanism

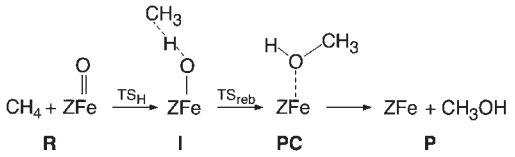

From the diagrams of Figures 5 and 6 it is apparent that the most striking difference between the quintet and triplet spin states is the reduced splitting of the α and β levels in the latter. This is because the lowering of the spin multiplicity from $S = 2$ to $S = 1$ makes the exchange field of the unpaired α-spin electrons less stabilizing. With regard to the reactivity, worth mentioning are the upshift of the α-d_{z^2} (σ^*) in the triplet, which then will less readily accept electrons from the C−H σ orbital, and the reduced gap between the α-d_{z^2} (σ^*) and the unoccupied β-spin Fe−O_{ax} π^* orbitals. Actually the lowest β-spin Fe−O_{ax} π^* orbital, the d_{xz}, is nearly degenerate with the α-d_{z^2} (σ^*) in ^{3}**1** and only 0.15 eV higher in ^{3}**2**, thus opening a π reaction pathway in the H-abstraction from methane.

Methane Hydroxylation by the Fe-ZSM-5 "α-oxygen" Model. In this section we present the results for the methane hydroxylation by the zeolite "α-oxygen" model, ZFeO, following the rebound mechanism shown in Scheme 1. This involves initial hydrogen abstraction from methane by ZFeO to yield ZeFeOH together with a methyl radical (intermediate **I**), followed by methyl radical rebound on the ferric-hydroxo intermediate, **I**, to generate the ferric-methanol complex, **PC**, which then releases the methanol and restores the unoxidized ZFe cluster.

The reaction path for the formation of methanol from methane and ZFeO was explored for the quintet and triplet spin states of isomer **1** and for the quintet spin state of isomer **2**, the triplet state of this isomer being too high in energy to play a role in the methane hydroxylation reaction.

First, we will focus on the reactivity of isomer **1** in the quintet ground spin state and in the triplet excited state. Then, we will compare the reactivity of the isomers **1** and **2** in their quintet ground spin state.

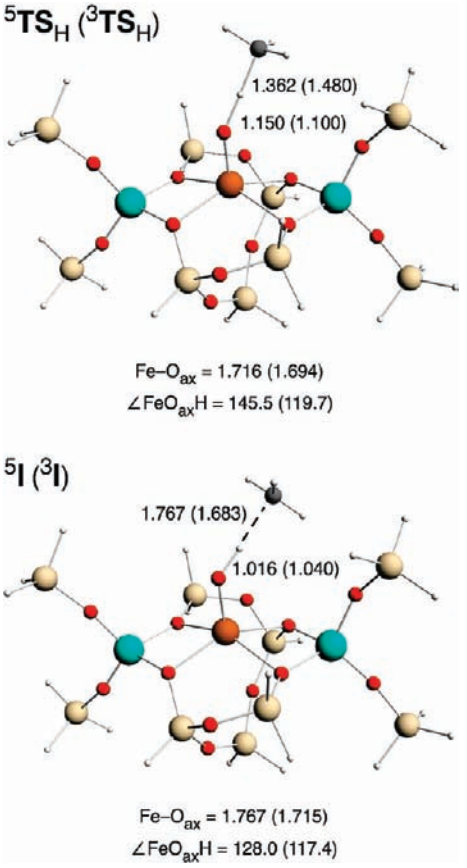

Figure 8. DFT/ZORA/BP86/TZ2P optimized geometries (Å and degrees) of the species involved in the H-abstraction from methane by ^{3,5}**1**.

Figure 7 shows the potential energy profiles for the methane hydroxylation reaction by ^{3,5}**1** computed at the DFT/ZORA/BP86/TZ2P level of theory. The relevant energy data computed for the methane hydroxylation reaction by ^{3,5}**1** and ^{5}**2** are collected in Table 3.

The key geometrical features of the species involved in the methane hydroxylation reaction by ^{3,5}**1** are shown in Figures 8 and 9, and in Figures S1−S4 in the Supporting

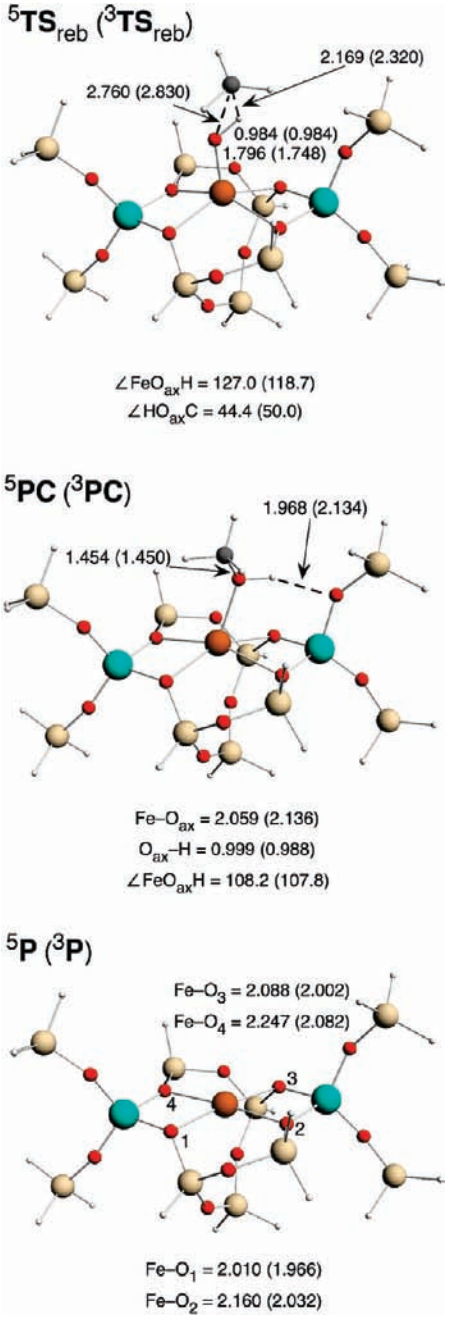

Figure 9. DFT/ZORA/BP86/TZ2P optimized geometries (Å and degrees) of the species involved in the rebound phase of methane hydroxylation by ^{3,5}**1**.

Information. The spin densities and charges computed for these species are reported in Table 4.

We consider first the methane hydroxylation path on the quintet spin surface, starting with H-abstraction. This step involves attack of methane on the catalyst leading to the transition state, ^{5}**TS**$_H$, without formation of a reactant complex, that is, a complex in which the oxo of ferryl is weakly bound to methane. The geometrical parameters in Figure 8 show that in ^{5}**TS**$_H$ the transferring hydrogen is closer to the oxygen atom than to the carbon ($d_{O\cdots H}$ = 1.15 Å and $d_{C\cdots H}$ = 1.36 Å), which means we are dealing with a rather late transition state. The spin density distribution in the TS shows already a quite pronounced radical character of the methyl. From the transition state geometry it is evident that not only the α-d$_{z^2}$ (σ*) but also the β-d$_{xz}$ orbital is involved as acceptor orbital: the 145.5° and 139.6° computed for the ∠FeOH angle at the BP86 and OPBE level, respectively, clearly indicate that the methane σ_{C-H} donor orbital seeks a compromise position between linear (180°), to optimize the overlap with the α-d$_{z^2}$ (σ*), and 90°, to optimize the overlap with the β-d$_{xz}$ MO (the $2\pi_x$* in Figure 1 is nominally the β-d$_{xz}$ MO; it is in fact a Fe-d$_{xz}$−O-2p$_x$ antibonding orbital, the σ_{C-H} donor orbital can maximize its overlap with the O-2p$_x$ by decreasing the angle to 90°).[19,20] This is different from the TS for the pentaaqua complex $(H_2O)_5$ FeO^{2+}(S = 2), where the TS is linear (∠FeOH angle ca. 180°), suggesting almost exclusive involvement of the α-d$_{z^2}$ (σ*). This predominance of the α-d$_{z^2}$ (σ*) and the linear TS cannot be explained completely by the lower energy of the α-d$_{z^2}$ (σ*): it is lower than $2\pi_x$*, but only by 0.28 eV (cf. Figure 1). Other factors—overlap of σ(C−H) with the α-d$_{z^2}$ (σ*) and $2\pi_x$* respectively, and steric repulsion effects—are also important in determining the relative importance of the σ* and π* channels.[19,20]

Relaxation of ^{5}**TS**$_H$ toward products leads to intermediate **I**, which has a Fe-bound hydroxo group (d_{Fe-OH} = 1.767 Å) weakly interacting with the methyl carbon ($d_{OH\cdots C}$ = 1.767 Å). The high spin density found on the methyl carbon (−0.87) indicates substantial radical character in the CH_3 fragment. The spin densities on the iron and axial oxygen atoms are also high, higher than in the transition state. At the DFT/ZORA/BP86/TZ2P level of theory the H-abstraction reaction (CH_4 + ^{5}**1** → ^{5}**TS**$_H$ → ^{5}**I**) has quite a low energy barrier of 6.6 kcal/mol and is endothermic by 6.5 kcal/mol. Comparable results are obtained at different levels of theory, as inferred from the $\Delta E^{\ddagger}_{TS_H}$ and ΔE_1 values gathered in Table 3. It is gratifying that the two different codes, ADF (STO basis functions) and Turbomole (Gaussian basis functions), give quite close results, and the same holds for the functionals BP86 and OPBE. Only in the final step toward the products the OPBE functional clearly gives a significantly larger lowering of the total energy. Intermediate **I** undergoes OH-rebound generating the product complex, ^{5}**PC**. During this step the hydroxyl group of the intermediate complex is transferred to the methyl carbon, yielding methanol. In the product complex the methyl alcohol remains coordinatively bound to the metal with the Fe···O distance ranging from 2.059 to 2.118 Å, depending on the functional and basis set used (see Figure 9 and Figures S3 and S4 in the Supporting Information). In ^{5}**PC** the hydroxyl hydrogen is engaged in a rather strong hydrogen bond with the closest oxygen atom of the zeolite framework, which induces significant changes in the iron coordination sphere. There is no evidence of such an intramolecular hydrogen bond interaction in the ^{5}**PC** structure obtained at the OPBE level (see Figure S4 in the Supporting Information), which is consistent with this functional failing to describe hydrogen bonds.[72] The energy data in Table 3 show that the rebound step is highly exothermic, ΔE_2 ranges from −38.7 to −44.5 kcal/mol, and has a very low energy barrier of ∼2 kcal/mol, indicating that OH-rebound is, as always, much faster than H-abstraction. We estimated the KIE for ^{5}**TS**$_H$ using the approximate Eyring expression based on ZPEs only. Substitution of all hydrogen atoms of methane by deuterium leads to KIE values ranging from 5.4 to 5.7, depending on the level of

Table 4. Atomic Spin Densities (ζ) and Charges (q) Computed at Different Levels of Theory for the Reaction Intermediates in the Rebound Mechanism of Methane-to-Methanol Oxidation by ^{3,5}**1**

	TS_H		I		TS_{reb}	PC		P	
	BP86[a]/BP86[b]	OPBE	BP86[a]/BP86[b]	OPBE	BP86[a]/BP86[b]	BP86[a]/BP86[b]	OPBE	BP86[a]/BP86[b]	OPBE
					^{5}**1**				
ζ_{Fe}	3.88/3.86	3.97	4.07/4.03	4.09	4.08/4.05	3.77/3.76	3.82	3.74/3.77	3.78
ζ_O	0.28/0.34	0.26	0.38/0.44	0.28	0.40/0.45	0.04/0.04	0.02	0.00/0.00	0.00
ζ_C	−0.51/−0.54	−0.51	−0.87/−0.89	−0.69	−0.92/−0.93	0.00/0.00	0.00/0.00	0.00/0.00	0.00
ζ_H	−0.02/−0.01	−0.03	−0.01/−0.02	−0.03	0.01/0.00	0.00/0.00	0.00/0.00	0.00/0.00	0.00
q_{Fe}	1.09/0.80	1.19	1.11/0.77	1.20	1.12/0.75	0.93/0.65	1.04	0.88/0.60	0.91
q_O	−0.50/−0.55	−0.55	−0.49/−0.57	−0.55	−0.49/−0.56	−0.53/−0.43	−0.56	−0.51/−0.44	−0.51
q_C	0.59/−0.44	0.60	0.47/−0.44	0.57	0.46/−0.40	0.90/−0.23	0.89	0.84/−0.18	0.80
q_H	0.15/0.31	0.20	0.18/0.33	0.21	0.15/0.32	0.28/0.37	0.25	0.21/0.30	0.23
					^{3}**1**				
ζ_{Fe}	2.51/2.52	2.62	2.58/2.59	2.73	2.59/2.58	2.01/2.01	2.07	2.04/2.09	2.08
ζ_O	0.04/0.06	−0.03	0.11/0.13	0.11	0.20/0.22	0.04/0.04	0.02	0.00/0.00	0.00
ζ_C	−0.65/−0.69	−0.67	−0.82/−0.86	−1.00	−0.94/−0.95	0.00/0.00	0.00/0.00	0.00/0.00	0.00
ζ_H	−0.02/−0.01	−0.03	−0.02/−0.02	−0.03	0.00/0.00	0.00/0.00	0.00/0.00	0.00/0.00	0.00
q_{Fe}	0.96/0.62	0.97	0.97/0.62	0.98	1.00/0.60	0.84/0.51	0.88	0.77/0.44	0.78
q_O	−0.46/−0.47	−0.47	−0.45/−0.47	−0.46	−0.45/−0.48	−0.51/−0.41	−0.54	−0.51/−0.44	−0.51
q_C	0.55/−0.44	0.56	0.48/−0.43	0.44	0.45/−0.42	0.90/−0.23	0.91	0.84/−0.18	0.80
q_H	0.18/0.33	0.26	0.19/0.33	0.24	0.15/0.33	0.26/0.34	0.23	0.21/0.30	0.23

[a] ADF (ZORA/TZ2P). [b] TURBOMOLE (def2-TZVP).

theory, at a temperature of 298.15 K. The calculated KIE values compare well with the ones obtained experimentally for methane versus methane-d_2 oxidation by "α-oxygen" for which, depending on the temperature, KIE values ranging from 1.9 to 5.5 were measured.[34]

To obtain the transition state geometry of the rebound step, TS_{reb}, we have first performed a potential energy scan along the intrinsic reaction coordinate, that is, the ∠HOC angle, the one describing the rotation of the methyl radical around the hydroxyl hydrogen to bind the oxygen.[12] The maximum energy structure was then taken as a guess for the transition state search. These calculations were performed using the BP86 functional. We were not able to perform a potential energy scan at the OPBE level because no structure could be optimized. ^{5}**TS**$_{reb}$ has a reactant-like structure with a short Fe−OH distance of 1.796 Å, long C···O and C···H distances of 2.760 and 2.169 Å, respectively, and a ∠HOC angle of 44.4°. Notably, the carbon atom does not lie on the FeOH plane, the ∠FeOHC dihedral angle being 134°. The displacement of the carbon atom out of the FeOH plane serves to maximize the overlap between the carbon $2p_z$ and the pertinent oxygen lone pair.

The reaction product, methanol, is released in a subsequent dissociative step, ^{5}**PC** → ^{5}ZFe + CH_3OH, with an energy cost of 23.8 kcal/mol (24.5 kcal/mol at the BP86/def2-TZVP level) relative to **PC**. At the OPBE level this step is less endothermic and costs 12.0 kcal/mol (this is the only instance of a significant difference between the BP86 and OPBE functionals in Table 3). Anyhow, the energy required for the desorption of methanol is quite high, which is in agreement with the statement of Panov et al.[34,87] that methanol is strongly bound to the zeolite surface and can be extracted only by using a mixture of water and acetonitrile. The energy required for methanol desorption can be provided at least in part, by the methane hydroxylation reaction itself which is highly exothermic on the quintet surface, ΔE ranges from −10.9 to −20.1 kcal/mol (see Table 3).

Desorption of the methanol affords the ZFe cluster in its quintet ground spin state and the metal in the 2+ oxidation state. The molecular and electronic structure data computed for this complex agree well with those previously reported by Kachurovskaya et al.[44]

Coming now to the reactivity on the low-spin surface, we note that the triplet surface lies above the quintet surface in the entrance channel of the oxidative process, especially at the OPBE level (see Table 2), and is highly destabilized during the complete reaction process thus making spin crossover largely unfavorable energetically. This is immediately apparent in Figure 7. The energy data in Table 3 show that the H-abstraction process on the triplet surface is much more endothermic, ΔE_1 ranges from 17.3 to 17.8 kcal/mol, and has a much higher energy barrier (more than 18 kcal/mol) than on the quintet surface. On account of the higher energy barrier, ^{3}**TS**$_H$ occurs later than ^{5}**TS**$_H$. According to the geometrical parameters in Figure 8 and Figures S1 and S2 in the Supporting Information, in ^{3}**TS**$_H$ the O···H distance is shorter and the C···H distance is longer than in ^{5}**TS**$_H$ (1.10 vs 1.15 Å and 1.48 vs 1.36 Å, at the DFT/ZORA/BP86/TZ2P level). This is also reflected in the spin density distribution showing a more pronounced radical character of the methyl in ^{3}**TS**$_H$. Comparison of the spin density distribution in ^{3}**TS**$_H$ and ^{3}**1** reveals that the transition state species involves a significant charge transfer from the methane toward the ferryl moiety. The charge transfer involves both the Fe−O σ antibonding MO, the α-d_{z^2} (σ*), and the Fe−O π antibonding MO, the β-d_{xz}. This is not surprising as these acceptor orbitals are nearly degenerate in ^{3}**1** (see diagram of Figure 5). In ^{3}**TS**$_H$ the ∠FeOH angle is 121°, much smaller than in ^{5}**TS**$_H$, indicating that the transition state geometry is largely controlled by the interaction of the C−H σ bond of the substrate with the

(87) Sobolev, V. I.; Dubkov, K. A.; Panna, O. V.; Panov, G. I. *Catal. Today* **1995**, *24*, 251.

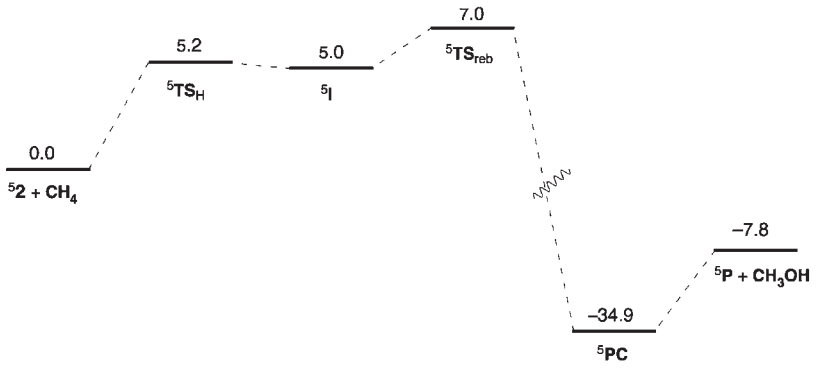

Figure 10. DFT/ZORA/BP86/TZ2P potential energy profiles for methane hydroxylation reaction by ^{5}**2**. Energies are in kcal/mol and include ZPE correction.

β-d$_{xz}$ ($2\pi_x$*) although there is also a significant α-σ_{C-H} donation into the α-d$_{z^2}$ (σ*). As discussed in detail by Michel and Baerends[20] the donation from the σ_{C-H} into the lowest vacant acceptor orbitals of the catalyst also controls the H-abstraction energy barrier: the lower the acceptor orbitals lie in energy the lower $\Delta E^{\ddagger}_{TS_H}$ is.[16,18] Thus, the huge increase of the H-abstraction energy barrier observed on going from the quintet to the triplet surface can be mainly traced to the difference in the energy of the acceptor orbitals of the electrophile. Because of the reduced α-exchange field, the α-d$_{z^2}$ (σ*) acceptor MO lies in ^{3}**1** at much higher energy than in ^{5}**1**. Also the $2\pi_x$* (β-d$_{xz}$) and $2\pi_y$* (β-d$_{yz}$) are higher in ^{3}**1**, but the difference is much less extreme for these d$_\pi$* orbitals. In this case the difference is not due to a difference in exchange field (the number of β-spin electrons actually increases), but the effect is indirect: because of the depletion of the antibonding α-d$_{x^2-y^2}$, the FeO$_{eq}$ bond distances contract (the effect is particularly large for Fe$-$O$_2$ and Fe$-$O$_4$, see Tables 1 and 2), and this drives the empty d$_\pi$* orbitals up.

Relaxation of ^{3}**TS**$_H$ toward products leads to intermediate ^{3}**I**. The intermediate complex has a Fe-bound hydroxyl group (d_{Fe-OH} = 1.715 Å) weakly interacting with the methyl carbon ($d_{OH\cdots C}$ = 1.683 Å), which shows almost a fully developed spin (ζ_C = $-$0.82). Subsequent OH-rebound through ^{3}**TS**$_{reb}$ leads to the product complex, ^{3}**PC**. The rebound step is highly exothermic (ΔE_2 ranges from $-$34.4 to $-$39.3 kcal/mol) although less than in the case of the quintet spin state. This is because ^{3}**PC** is less stable than ^{5}**PC** because of a less effective interaction between methanol and iron in the former. The Fe$\cdots$O distance is indeed in ^{3}**PC** longer than in ^{5}**PC** (2.136 vs 2.059 Å, at the DFT/ZORA/BP86/TZ2P level). The rebound step is also on the low spin surface very fast ($\Delta E^{\ddagger}_{TS_{reb}}$ 3.5$-$3.37 kcal/mol), although the barrier is a little higher than on the quintet surface. The important point here is that regardless of the spin state OH-rebound is much more facile than the H-abstraction, both at the thermodynamic and kinetic levels. As can be inferred from Figure 9 and Figure S3 in the Supporting Information, the salient structural features of ^{3}**TS**$_{reb}$ do not differ significantly from those of ^{5}**TS**$_{reb}$ save for a larger $\angle$HOC angle (50.0$-$53.2°) and a smaller $\angle$FeOHC dihedral angle (111.8$-$114.4°).

The release of methanol from ^{3}**PC** is energetically more favorable than from ^{5}**PC** as it requires an energy amount ranging from 5.5 kcal/mol (DFT/ZORA/OPBE/TZ2P) to 15.3 kcal/mol (DFT/BP86/def2-TZVP). The more facile desorption of methanol from ^{3}**PC** is consistent with the methanol being in ^{3}**PC** less bound than in ^{5}**PC**, as pointed out above.

According to the values in Table 3 the overall methane hydroxylation reaction is exothermic also on the triplet surface, although much less than on the quintet surface. Our results are at variance with previous theoretical results by Yoshizawa et al.[43] according to which the methane hydroxylation reaction by "α-oxygen" of Fe-ZSM-5 zeolite is highly endothermic. However, the results of these authors are for $[FeO]^+$ instead of $[FeO]^{2+}$ as the active catalytic center, which, as pointed out before, is expected to give much higher barriers.

Finally, we examine the reactivity of isomer **2** on the quintet ground state surface. Figure 10 shows the potential energy profile for the methane hydroxylation reaction by ^{5}**2** computed at the DFT/ZORA/BP86/TZ2P level. The key geometrical features of the species involved in the reaction path are displayed in Figures 11 and 12 and in Figures S5 and S6 in the Supporting Information. The spin densities and charges computed for these species are reported in Table 5.

The energy profiles for the methane hydroxylation reaction by ^{5}**2** and ^{5}**1** are very similar. The reaction starts with the attack of methane on the catalyst leading to the transition state, ^{5}**TS**$_H$ (**2**), without formation of a reactant complex. Relaxation of ^{5}**TS**$_H$ (**2**) toward products leads to intermediate ^{5}**I** (**2**). From the ΔE_1 and $\Delta E^{\ddagger}_{TS_H}$ values gathered in Table 3 it is apparent that the H-abstraction step is more facile for ^{5}**2** than for ^{5}**1**, both at the thermodynamic and kinetic levels. On account of the lower energy barrier, ^{5}**TS**$_H$ (**2**) occurs earlier than ^{5}**TS**$_H$ (**1**).

The geometrical parameters in Figure 11 and Figures S5 and S6 in the Supporting Information show, indeed, that in ^{5}**TS**$_H$ (**2**) the transferring hydrogen is almost midway between C and O ($d_{C\cdots H}$ = 1.292 Å, $d_{O\cdots H}$ = 1.210 Å, at the DFT/ZORA/BP86/TZ2P level). That ^{5}**TS**$_H$ (**2**) occurs earlier than ^{5}**TS**$_H$ (**1**) is also evident from the spin density distribution in Table 5 showing a less pronounced radical character of the carbon atom of the methyl group in the former. Similar to ^{5}**TS**$_H$ (**1**), ^{5}**TS**$_H$ (**2**) settles for a compromise geometry that allows interaction of the methane σ_{C-H} donor orbital with both the acceptor MOs of the catalyst by assuming an $\angle$FeOH angle of

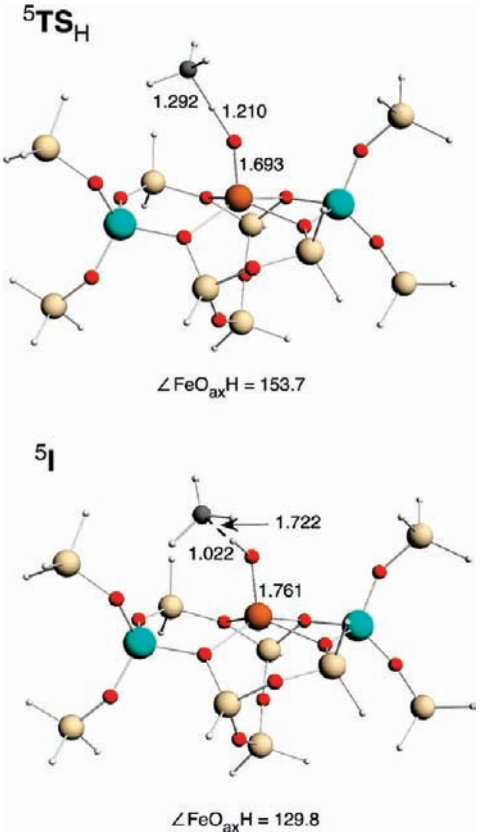

Figure 11. DFT/ZORA/BP86/TZ2P optimized geometries (Å and degrees) of the species involved in the H-abstraction from methane by ^{5}**2**.

153.7° (141.8° at the OPBE level), very similar to the 145.5° for ^{5}**TS**$_H$ (**1**).

The small lowering of the H-abstraction barrier going from ^{5}**1** to ^{5}**2**, from 6.6 to 5.2 kcal/mol, and the subtle molecular and electronic structure differences between ^{5}**TS**$_H$ (**1**) and ^{5}**TS**$_H$ (**2**) as well, can be traced primarily to small differences in energy and composition of the lowest acceptor MOs in the two isomers. As a matter of fact, the main acceptor MO, the α-d$_{z^2}$ (σ*), is in ^{5}**2** ∼ 0.2 eV lower than in ^{5}**1**. In turn, the β-d$_{xz}$ lies at about the same energy in the two isomers, but has in ^{5}**2** a higher oxo character than in ^{5}**1** (39% vs 36%).

The change of the metal coordination mode has a very minor influence on the rebound step, as can be inferred from the $\Delta E^{\ddagger}_{TS_{reb}}$ and ΔE_2 values reported in Table 3 for ^{5}**1** and ^{5}**2**. Thus, H-abstraction is also for ^{5}**2** the rate-determining step. Also the KIE value estimated for ^{5}**TS**$_H$ (**2**) is not so different from the one computed for ^{5}**TS**$_H$ (**1**). Substitution of all hydrogen atoms of methane by deuterium leads, indeed, to a KIE value ranging from 4.9 to 5.1, depending on the level of theory. Notably, the KIE value computed for methane versus methane-d$_2$ oxidation, which is more comparable to the experiment,[34] is 4.7 at the DFT/ZORA/BP86/TZ2P level.

Release of methanol from ^{5}**PC** (**2**) is energetically more demanding than from ^{5}**PC** (**1**) (27.1 vs 23.8 kcal/mol, at the DFT/ZORA/BP86/TZ2P level). This is because ^{5}ZFe (**2**) is slightly less stable than ^{5}ZFe (**1**). For the same reason the overall methane hydroxylation reaction is less exothermic in the case of ^{5}**2** than in the case of ^{5}**1** (−7.8 vs −10.9 kcal/mol, at the DFT/ZORA/BP86/TZ2P level).

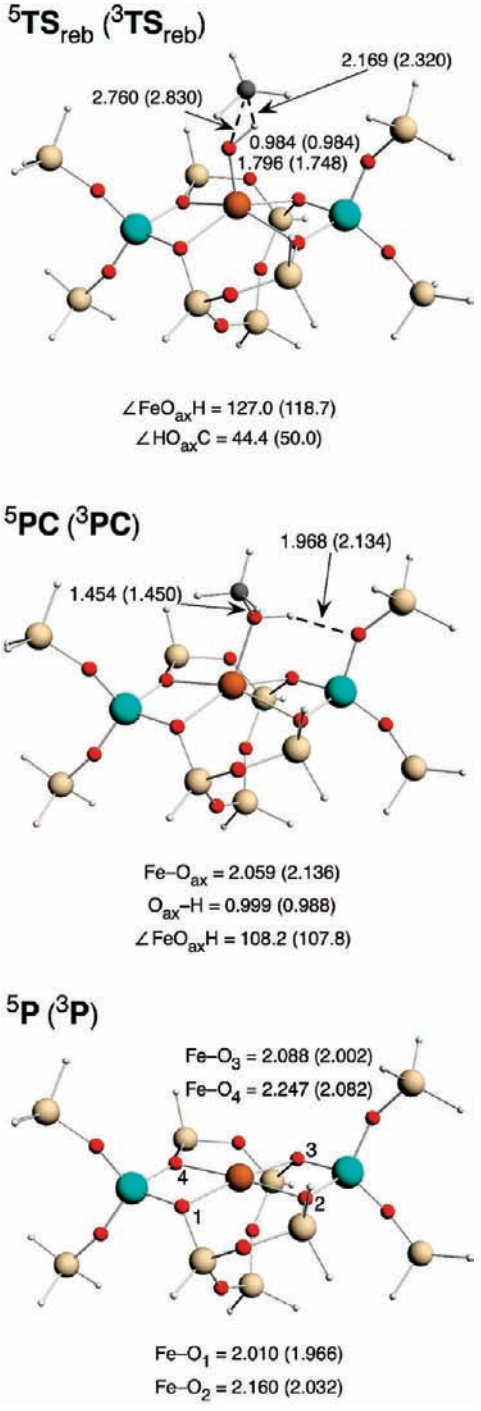

Figure 12. DFT/ZORA/BP86/TZ3P optimized geometries (Å and degrees) of the species involved in the rebound phase of methane hydroxylation by ^{5}**2**.

In summary, our theoretical results suggest that the rebound mechanism is a feasible pathway for methane oxidation by ZFeO. The calculations show that the triplet state of the oxo species, ^{3}**1**, can hardly be involved in C−H activation. By contrast, the reaction proceeds with very low barriers on the quintet surface of either **1** or **2** isomers, although the barrier for H-abstraction, which is the rate-determining step, is slightly lower for the isomer **2**.

Table 5. Atomic Spin Densities (ζ) and Charges (q) Computed at Different Levels of Theory for the Reaction Intermediates in the Rebound Mechanism of Methane-to-Methanol Oxidation by ^{5}**2**

	TS_H		I		TS_{reb}	PC		P	
	BP86[a]/BP86[b]	OPBE	BP86[a]/BP86[b]	OPBE	BP86[a]/BP86[b]	BP86[a]/BP86[b]	OPBE	BP86[a]/BP86[b]	OPBE
					^{5}**2**				
ζ_{Fe}	3.77/3.77	3.90	4.05/4.00	4.15	4.05/4.00	3.78/3.77	3.83	3.72/3.74	3.76
ζ_O	0.30/0.33	0.25	0.37/0.43	0.41	0.39/0.42/	0.03/0.03	0.01	0.00/0.00	0.00
ζ_C	−0.39/−0.44	−0.43	−0.83/−0.86	−1.00	−0.85/−0.86	0.00/0.00	0.00/0.00	0.00/0.00	0.00
ζ_H	−0.03/−0.02	−0.04	−0.02/−0.02	−0.02	0.01/0.00	0.00/0.00	0.00/0.00	0.00/0.00	0.00
q_{Fe}	1.07/0.84	1.17	1.09/0.81	1.21	1.09/0.78	0.93/0.73	1.01	0.91/0.71	0.92
q_O	−0.50/−0.52	−0.55	−0.50/−0.56	−0.54	−0.51/−0.54	−0.54/−0.45	−0.56	−0.51/−0.44	−0.51
q_C	0.61/−0.45	0.61	0.46/−0.43	0.43	0.49/−0.39	0.90/−0.21	0.88	0.84/−0.18	0.80
q_H	0.12/0.30	0.17	0.17/0.33	0.20	0.17/0.33	0.28/0.37	0.28	0.21/0.30	0.23

[a] ADF (ZORA/TZ2P). [b] TURBOMOLE (def2-TZVP).

IR Spectra of Intermediate Species. Panov et al.[88] postulated the formation of $FeOCH_3$ species on the basis of the IR spectrum obtained by treatment of (activated) zeolite with methane. The IR spectrum shows in the C−H stretching region four bands at 2823, 2919, 2945, and 2964 cm^{-1}, the last two very broad and weak.

In the same spectrum in the O−H stretching region an intense band at 3674 cm^{-1} was observed, which led these authors to postulate the formation of a FeOH species.

It is important to realize that formation of these two species can be easily rationalized if the intermediate complex formed after H-abstraction (^{5}**I**) first breaks down into ZFeOH and free $CH_3^{\bullet}$. The methyl radical then may attack another α-site collapsing into the methoxy species. Dissociation of the intermediate is endothermic, the amount of energy required depending on the system at hand. In our case it costs, at the BP86/TZ2P level, upon ZPE inclusion, 4.8 kcal/mol for the isomer **2**. This value is obtained considering ZFeOH in the sextet ($S = 5/2$) ground spin state antiferromagnetically coupled to the $S = -1/2$ $CH_3^{\bullet}$ radical (if one considers ZFeOH in the energetically higher $S = 3/2$ spin state coupled to a parallel $S = 1/2$ $CH_3^{\bullet}$ radical the dissociation reaction costs 20.0 kcal/mol). In turn, the reaction ZFeO (^{5}**2**) + $CH_3^{\bullet} \rightarrow$ $ZFeOCH_3$ ($S = 5/2$) is exothermic by 73.3 kcal/mol (ZPE included). (N. B.: in $ZFeOCH_3$ the Fe−O−C angle is 148°). Thus, the intermediate complex may evolve toward dissociation (4.8 kcal/mol) or undergo oxygen rebound (TS barrier = 2.0 kcal/mol), the latter process being slightly favored energetically.

We have also computed the IR spectra of ZFeOH ($S = 5/2$) and $ZFeOCH_3$ ($S = 5/2$). For ZFeOH we find an O−H stretching vibration at 3603 cm^{-1}, that is, sufficiently close to the 3674 cm^{-1} value experimentally found to support the experimental assignment. For $ZFeOCH_3$, we find only 3 IR active C−H vibration modes around 2900 cm^{-1}, at 2888, 2967, and 2971 cm^{-1}, of very weak and comparable intensity. Although the fourth experimental band at 2945 cm^{-1} could well be an overtone band, as suggested by Panov et al.,[88] the correspondence with the experiment is not so good in the case of $ZFeOCH_3$. Interestingly, the IR spectrum computed for the **PC** (isomer **2**) complex (see Figure 12) shows instead four bands in the C−H stretching region: 2947, 3027, 3050, and 3064 cm^{-1} with the last two remarkably more intense than the first two. An analysis of these normal modes reveals that the first three vibrations are associated to the C−H stretching modes of the methanol in **PC**, the fourth is associated to the stretching of the O−H group; this stretching is much red-shifted relative to the bare methanol (3681 cm^{-1}) because of the weakening of the O−H bond caused by the hydrogen bonding with the oxygen atom of the zeolite, see Figure 12.

In conclusion, the C−H stretching region of the experimental IR spectrum does not unequivocally prove the existence of an $FeOCH_3$ moiety, but it may arise from the **PC** of the rebound mechanism, or from contributions of both **PC** and $ZFeOCH_3$.

Conclusions

We conclude that the reactivity of the α-oxygen site of Fe-ZSM-5 can be fully explained as a consequence of an optimal ligand environment for the $[FeO]^{2+}$ species offered by the cation exchange site of the zeolite. Notably, it offers an equatorial set of oxygen donor ligands, which is weak enough to keep the Fe in the high-spin configuration. This is advantageous for a low energy of the α spin LUMO, the α-d_{z^2} (σ^*), which is, with oxygen donor ligands, the most important acceptor orbital. In the second place, there is the rather unique circumstance in this particular site for FeO^{2+} that it does not have a *trans* axial donor ligand. This is in conformance with the ideal situation as proposed in ref 16 which is approximately realized with the coordination of EDTA to FeO^{2+}.[16]

We have given arguments to favor the d^4 Fe(IV) metal state, that is, a $Fe^{IV}O^{2+}$ moiety, as active center. This is at variance with the interpretation of experimental data from Mössbauer spectra[23] and from resonant inelastic X-ray scattering (RIXS),[49,50] which favor a Fe^{3+} metal, that is, a quasi-radical $[Fe^{III}O^{\bullet-}]^{2+}$ electronic structure. We wish to caution, however, that the iron charge and the oxygen radical character of the FeO^{2+} moiety are very difficult to establish unequivocally. In a sense we always have radical character, since the systems are open shell anyway. It is from the calculations impossible to say whether the electronic structure is better described as $[Fe(III)O^{\bullet-}]^{2+}$ than as $[Fe^{IV}O^{2-}]^{2+}$, since the orbitals are not purely Fe-3d or O-2p, but are strong mixtures.[10] The calculations do show considerable

(88) Panov, G. I.; Dubkov, A.; Paukshtis, Y. A. In *Catalysis by Unique Metal Ion Structures in Solid Matrices - NATO Science Series, II. Mathematics, Physics and Chemistry*; Centi, G., Wichterlova, B., Bell, A. T., Eds.; Kluwer Academic Publishers: Dordrecht, 2001; Vol. *13*; pp 149.

delocalization of the spin onto the oxo oxygen, which is of course far from the O^{2-} electronic configuration of the formal $Fe^{IV}O^{2-}$ picture. The Fe in the orbital scheme of Figure 1 may be formally Fe^{IV}, but of course the charge on Fe in the complexes is far from +4 (more like +1, see Tables). It is possible that the experimental results can be explained just as well on the basis of our proposed electronic configuration as displayed in Figure 1. The crucial point is that a $[Fe(III)O^{\bullet-}]^{2+}$ picture for the electronic configuration has led to the assumption of occupation of the $3\sigma^*$, compare Figure 2 of ref 48 which is definitely contrary to our understanding of how FeO^{2+} acts in oxidation catalysis. Notably, a d^5 Fe(III) high spin electronic configuration, as is implied in the $[Fe(III)O^{\bullet-}]^{2+}$ description of the electronic structure, and which would be present in the FeO^+ moiety, would necessarily have the α-d_{z^2} (σ^*) orbital occupied, inhibiting its action as acceptor orbital. It therefore should exhibit much higher barriers, that is, lower reactivity. This is borne out by calculations.

The identification of the high-valent $[Fe^{IV}O^{2-}]^{2+}$ moiety as the active species also in the α-oxygen site of Fe-ZSM-5 brings this system in line with the well-known and much studied biological systems where the ubiquitous $[Fe^{IV}O^{2-}]^{2+}$ moiety appears to be the key active species in oxidation and hydroxylation reactions. In all cases the rebound mechanism[52,53,89] appears to be operative. It is interesting to note that this mechanism is in agreement with the experimental results on the simultaneous production of FeOH and $FeOCH_3$ upon reaction of methane with the α-oxygen sites by Panov et al.,[88] since there is evidence that these are often produced from binuclear Fe oxygen configurations. The $CH_3^{\bullet}$ radical formed in the H-abstraction step may react in the rebound step with the formed FeOH, but also with the nearby FeO^{2+} to form $FeOCH_3$.

Acknowledgment. A.R. and G.R. acknowledge financial support by the Università della Basilicata, Italy (RIL Funds 2006). E.J.B. was supported by WCU (World Class University) program through the Korea Science and Engineering Foundation funded by the Ministry of Education, Science and Technology (Project No. *R*32-2008-000-10180-0) and by the Dutch National Research School Combination "Catalysis by Design".

Supporting Information Available: Additional details are given in Figures S1−S8. This material is available free of charge via the Internet at http://pubs.acs.org.

(89) Groves, J. T. *J. Inorg. Biochem.* **2006**, *100*, 434.